A&A manuscript no.
(will be inserted by hand later)

Your thesaurus codes are:
02.04.1 - 08.09.3 - 08.14.1

ASTRONOMY
AND
ASTROPHYSICS
16.8.1996

Electron $\nu\bar{\nu}$ bremsstrahlung in a liquid phase of neutron star crusts

P. Haensel[1], **A.D. Kaminker**[2] **and D.G. Yakovlev**[2]

[1] N. Copernicus Astronomical Center, Polish Academy of Sciences, Bartycka 18, 00-716 Warszawa, Poland
[2] A.F. Ioffe Institute of Physics and Technology, 194021 St.Petersburg, Russia

Received ....; accepted ....

Abstract. Neutrino emissivity from the electron $\nu\bar{\nu}$ bremsstrahlung in the liquid layers of the neutron star crusts is studied. Nuclear composition of matter in neutron star crusts is considered for various scenarios of neutron star evolution. For the deep layers of the crust, the compositions of cold catalyzed matter, accreted matter and hot matter ($T \gtrsim 5 \times 10^9$ K) are shown to be very different, and this implies differences in the neutrino emissivity at given density and temperature. Neutrino-pair bremsstrahlung, due to collisions of relativistic degenerate electrons in a Coulomb liquid of atomic nuclei, is considered. The neutrino energy loss rate is expressed in a simple form through a Coulomb logarithm L – a slowly varying function of density, temperature, and nuclear composition. Non-Born corrections, thermal width of electron Fermi sphere, and finite sizes of nuclei are taken into account. Implications for cooling of neutron stars are discussed.

1. Introduction

A neutron star crust extends from the stellar surface to the internal core, up to densities of about 10^{14} g cm^{-3}. The properties of crustal matter are most important for studying neutron star physics and observational data (surface thermal X-ray emission, X-ray burst phenomena, evolution of magnetic fields, etc.). This article has two goals. First, we analyze nuclear composition of matter in neutron star crusts. Second, we reconsider the neutrino-pair bremsstrahlung (NPB) in liquid phase of the matter due to scattering of electrons on atomic nuclei,

$$e + (Z, A) \rightarrow e + (Z, A) + \nu + \bar{\nu}. \qquad (1)$$

NPB is known to be one of the most powerful mechanisms of neutrino emission in matter with density lower than the nuclear density, $\rho_0 = 2.7 \times 10^{14}$ g cm^{-3}.

Send offprint requests to: P. Haensel

NPB was considered in a number of works (see Itoh et al. 1989, and references therein). Let us mention detailed studies of Festa & Ruderman (1969), Flowers (1973), Dicus et al. (1976), Soyeur & Brown (1979), Itoh & Kohyama (1983), and Itoh et al. (1984a) who analyzed NPB due to electron scattering in liquid and crystalline dense matter. Pethick & Thorsson (1994) have shown that the band structure effects of electrons in solid matter drastically suppress the static lattice contribution to NPB. Finally, the reconsideration of the neutrino energy loss rate due to the electron-phonon scattering in the crystal phase was recently performed by two of us (see Yakovlev & Kaminker 1996).

In the present paper, we will reconsider the problem of the calculation of the neutrino losses from NPB in the hot neutron star crusts. We will restrict ourselves to the case of a liquid phase of the crust (temperature above melting temperature at given density). The actual nuclear composition of the crust depends on the formation scenario. In contrast to previous studies, our calculations will be performed for realistic models of nuclear composition, which are based on specific assumptions about the formation of the neutron star envelope.

The paper is organized as follows. In Sect. 2 we analyze physical conditions and nuclear composition of neutron star crusts. We discuss those differences between various neutron star crusts, which are important for the NPB emissivities. In Sect. 3 we recalculate the NPB energy generation rate for degenerate relativistic electrons and Coulomb liquid of atomic nuclei. Contrary to the previous works, we include the non-Born corrections and the effects associated with thermal width of the electron Fermi sphere. We express our results in a simple form – through a Coulomb logarithm, which is a slowly varying function of density, temperature, and nuclear composition of matter. In Sect. 4 we discuss NPB for various models of matter in neutron star crusts, and indicate possible implications of our results. General formalism of NPB is presented in Appendix A, mathematical aspects of the thermal broadening of electron Fermi sphere are considered in Appendix B. Dynamic screening of the electron-nucleus interaction is outlined in Appendix C.

2. Composition of neutron star crusts

2.1. Physical conditions

Consider dense matter of a neutron star crust in a density range 10^6 g cm$^{-3} \ll \rho \lesssim 10^{14}$ g cm^{-3}. If $\rho < \rho_{\rm ND} \simeq (4-6)\times 10^{11}$ g cm^{-3}, matter is composed of bare atomic nuclei (complete pressure ionization) immersed in an almost ideal gas of relativistic degenerate electrons. This phase of matter constitutes the *outer crust* of a neutron star. Above the neutron drip density, $\rho_{\rm ND}$, some fraction of neutrons is not bound in nuclei, and matter is composed of nuclei, immersed in the electron and neutron gases. The actual value of $\rho_{\rm ND}$ is weakly model dependent. It depends also on the scenario of formation of the neutron star crust. At $\rho \gtrsim 10^{14}$ g cm^{-3}, the topology of the nucleon distribution can be very different from the standard one (e.g., neutron gas bubbles in nuclear matter with a large neutron excess, see Lorenz et al. 1993 and references therein). Finally, for $\rho > \rho_{\rm h} \simeq 1.5\times 10^{14}$ g cm^{-3}, nucleons form a single, homogeneous phase. Note that the quoted value of $\rho_{\rm h}$ obtained recently by Lorenz et al. (1993) is significantly lower than the standard one, based on earlier calculations (Shapiro & Teukolsky 1983). Matter with $\rho_{\rm ND} < \rho < \rho_{\rm h}$ forms an *inner crust.*

The state of degenerate electrons in a neutron star crust is described by the electron Fermi-momentum $p_{\rm F}$ or relativistic parameter x

$$p_{\rm F} = \hbar(3\pi^2 n_e)^{1/3}, \qquad x = \frac{p_{\rm F}}{mc} \approx 1.009 \left(\frac{\rho_6}{\mu_e}\right)^{1/3}, \qquad (2)$$

where μ_e is the number of baryons per electron, and ρ_6 is density in units of 10^6 g cm^{-3}. The electron degeneracy (Fermi) temperature is

$$T_{\rm F} = T_0\,(\sqrt{1+x^2}-1), \;\; T_0 = \frac{mc^2}{k_{\rm B}} \approx 5.930\times 10^9 \text{ K}. \quad (3)$$

We will consider strongly degenerate electrons, $T \ll T_{\rm F}$.

The state of the nuclei (ions) is defined by the Coulomb coupling parameter

$$\Gamma = \frac{Z^2 e^2}{a k_{\rm B} T} \approx 0.2254 \frac{Z^{5/3}}{T_8} x, \qquad (4)$$

where Ze is the nucleus charge, $a = [3/(4\pi n_i)]^{1/3}$ is the ion-sphere radius, and T_8 is temperature in 10^8 K. At high temperatures, when $\Gamma \ll 1$, the nuclei constitute a Boltzmann gas. At lower T (higher Γ) the gas gradually (without any phase transition) transforms into a Coulomb liquid. The liquid solidifies (forms a Coulomb crystal) at $T = T_m$. For a classical one-component plasma of nuclei, $T_{\rm m} \approx 1.32\times 10^5 Z^{5/3}(\rho_6/\mu_e)^{1/3}$ K corresponds to $\Gamma = 172$ (Nagara et al. 1987). For high densities and light nuclei, the crystallization may be affected by zero-order quantum vibrations of nuclei (Mochkovitch & Hansen 1979, Chabrier 1993).

2.2. Models of matter in a crust

If $T \lesssim 5\times 10^9$ K $\simeq T_0$, one can approximate the composition of the crust by that calculated at $T=0$. Finite temperature corrections at $T \sim 10^9$ K result in the presence of a very small fraction of free neutrons even at $\rho < \rho_{\rm ND}$, with a negligible effect on the bulk composition of matter.

The compositions of the outer and inner crusts depend on the scenario of formation of these outer layers. We consider three models of matter in a neutron star crust. The first model is based on the assumption that matter is in its ground state (*cold catalyzed matter*). The second one is the model of *accreted matter* valid when the neutron star accreted a sufficient amount of matter during its life. Both models are appropriate for $T \lesssim 5\times 10^9$ K. In both cases the nuclei are assumed to constitute a one-component plasma (A, Z), which behaves either as a Coulomb liquid ($T > T_{\rm m}$) or as a Coulomb body-centered cubic crystal ($T < T_{\rm m}$). In addition we consider (Sect. 2.4) the model of *hot matter* valid for $T \gtrsim 5\times 10^9$ K.

Some uncertainties in calculations of nuclear composition come from extrapolation of the laboratory nuclear physics to very large neutron excesses and huge pressures in neutron star crusts. These uncertainties are more important for the inner crust, and they increase with increasing ρ.

2.3. Cold catalyzed and accreted matter, $T \lesssim 5\times 10^9$ K

Let us first consider the models of cold catalyzed and accreted matter in the *outer crust* ($\rho < \rho_{\rm ND}$).

At finite temperature the first model corresponds to a complete thermodynamic equilibrium. This assumption is certainly valid at $T \gtrsim 10^{10}$ K (neutron star birth); its validity is extrapolated to the later stages of neutron star cooling. This determines the composition at a given pressure (density). In our analysis of the outer crust, we use the model of Haensel & Pichon (1994) based on the most recent experimental data on neutron rich nuclei.

The model of accreted matter represents the case, in which matter *is not* in the ground state. At typical accretion rates onto a neutron star in a close binary system, freshly accreted hydrogen-rich matter burns into helium. The latter, in turn, burns explosively into ^{56}Ni, which transforms eventually into ^{56}Fe. The products of thermonuclear burning are subsequently compressed under the weight of accreted matter at relatively low temperature. For instance, at the accretion rate $\sim 10^{-10}\ M_\odot$/yr typical temperature within the crust is a few times of 10^8 K. Accordingly the only further nuclear processes in the steadily formed 'new outer crust' are electron captures, which eventually lead to neutron drip at $\rho_{\rm ND} \simeq 6 \times 10^{11}$ g cm^{-3} (e.g., Haensel & Zdunik 1990). Note, that at the accretion rate 10^{-10} $M_\odot$/yr it takes 10^5 yr to replace the original outer crust, built of catalyzed (ground state) matter, by the new one.

The compositions of the accreted and cold catalyzed outer crusts are vastly different. At $\rho \simeq 10^{11}$ g cm^{-3} the values of Z and A in the accreted matter are less than half of those in the ground state. For instance, at the neutron drip we have Z=18, A=56 for the accreted matter (Haensel & Zdunik 1990) and Z=35, A=118 for the cold catalyzed matter (Haensel & Pichon 1994). The neutron drip density, which separates the *outer* and *inner* crusts, is rather insensitive to the scenario of the outer crust formation (cold catalyzed matter or accreted matter) and/or to the model of nuclei present in the matter. Irrespectively of the model, one gets $\rho_{\rm ND} = (4-6) \times 10^{11}$ g cm^{-3} (Shapiro & Teukolsky 1983, Haensel et al. 1989, Haensel & Zdunik 1990).

Now consider the models of ground state and accreted matter in the *inner crust* ($\rho > \rho_{\rm ND}$). In both cases we assume that (for $\rho \lesssim 10^{14}$ g cm^{-3}) matter is composed of spherical, neutron rich nuclei (A, Z) immersed in the electron and neutron gases. Because of relatively low temperature, the only processes involved in the formation of the "inner accreted crust" are electron captures, neutron emission and absorption, and pycnonuclear fusion.

For the ground state matter at $\rho > \rho_{\rm ND}$, we use the results of Negele & Vautherin (1973). The model of accreted crust is taken from Haensel & Zdunik (1990). We have constructed a specific model of an accreted crust for a neutron star which accreted 6×10^{-4} $M_\odot$. The bottom of the accreted layer is found at $\rho \simeq 1.1 \times 10^{13}$ g cm^{-3}.

Both models are developed for a one component plasma (single A, Z nuclide at a given pressure). This implies the onion structure of the crust, with fixed values of A, Z within certain pressure intervals.

Figures 1 and 2 present the relevant parameters of the ground state and accreted crusts versus density. The discontinuities in the values of (A, Z) are due to the shell and pairing effects in the binding energies of nuclei. Notice a strong dependence of Z^2/A (which is important for NPB, Sects. 3 and 4) on the crust formation scenario for 10^9 g cm^{-3} $\lesssim \rho \lesssim 10^{13}$ g cm^{-3}. The values of Z^2/A for the accreted crust are about $2-3$ times lower than for the ground state. The differences of the melting temperature are even higher (a factor of ~ 6 at $\rho \sim 10^{12}$ g cm^{-3}, Fig. 2). The melting temperature of the ground state matter for $\rho > 10^{12}$ g cm^{-3} is $\gtrsim 5 \times 10^9$ K. At such temperatures the thermal corrections to the composition of matter become important.

Let us notice that in the case of accreted crust at $\rho > 10^{10}$ g cm^{-3}, the ion plasma temperature, $T_{\rm p} = \hbar\omega_{\rm p}/k_{\rm B} = (\hbar/k_{\rm B})(4\pi Z^2 e^2 n_{\rm i}/m_{\rm i})^{1/2}$, where $n_{\rm i}$ is the number density of nuclei (ions) and $m_{\rm i}$ is their mass, becomes larger than the melting temperature of *classical* plasma. This seems to indicate, that corrections to $T_{\rm m}$, resulting from quantum (zero–point) vibrations of nuclei, might become significant. However, a quantitative analysis, based on the formulae derived by Chabrier (1993) (who corrected formulae obtained by Mochkovitch & Hansen (1979)) shows, that even in the most extreme cases, corresponding to minima of $T_{\rm m}$ at $\rho \gtrsim 10^{12}$ g cm^{-3} (see Fig. 2), quantum corrections to $T_{\rm m}$ were about a few percent. In the case of the ground state of matter we have always $T_{\rm p} < T_{\rm m}$, and so the quantum corrections to $T_{\rm m}$ are even smaller.

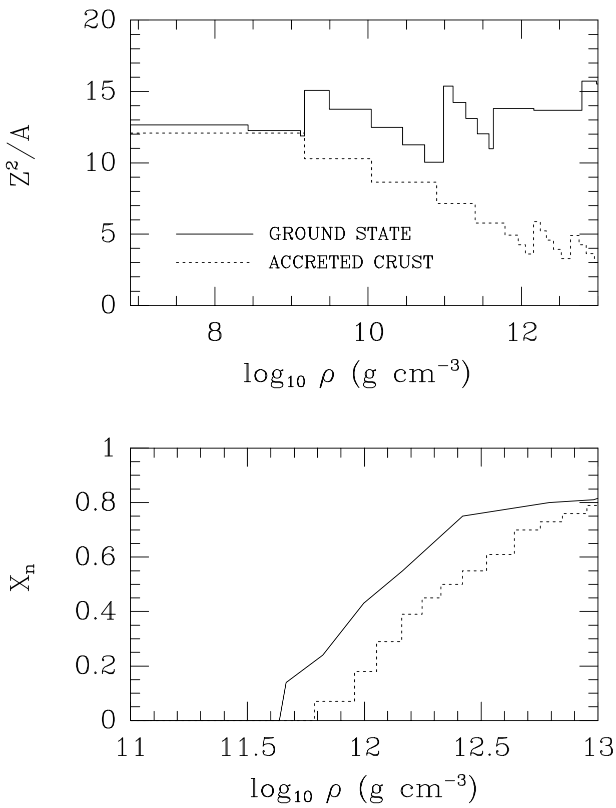

Fig. 1. Nuclear factor Z^2/A, important for NPB, and the mass fraction of free neutrons, $X_{\rm n}$ (related to mass fraction of atomic nuclei, X_A, by $X_A = 1 - X_{\rm n}$), versus density ρ (in g cm^{-3}), for two models of neutron star crust. Solid line: ground state of matter; dotted line: accreted crust.

2.4. Hot matter, $T \gtrsim 5 \times 10^9$ K

For $T > 5 \times 10^9$ K, the thermal effects strongly modify the nuclear composition. Both shell and pairing effects are washed out from the abundances of nuclei. Also, reshuffling of nucleons is no longer blocked efficiently by Coulomb barriers, and one can assume complete thermal equilibrium. We treat hot matter as a mixture of neutrons, protons, electrons, positrons and nuclei. In addition, we

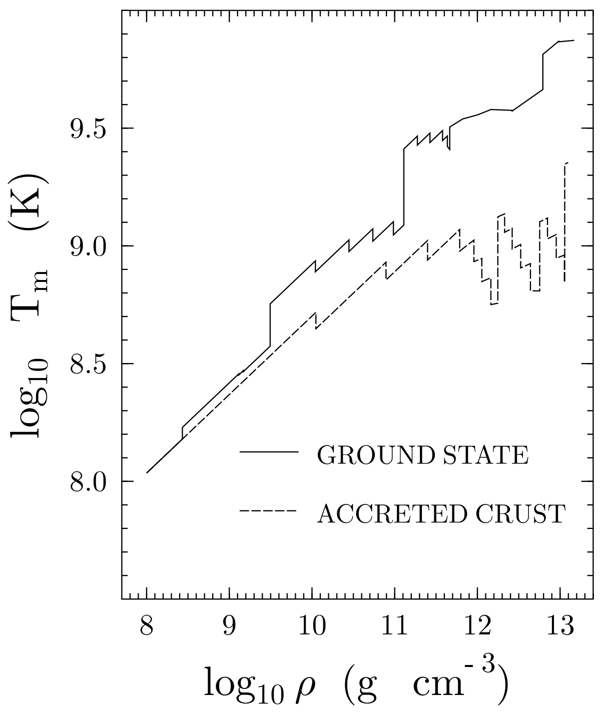

Fig. 2. Melting temperature T_m (K), versus density (in g cm^{-3}), for the same models as in Fig. 1.

represent light nuclei by the α particles, and heavy nuclei by a single species (A, Z) (e.g., Burrows & Lattimer 1984).

We describe the nuclei in hot dense matter, using the model of Lattimer & Swesty (1991), with a specific choice of the equilibrium incompressibility of nuclear matter, $K_s = 180$ MeV. We assume nuclear equilibrium, as well as beta equilibrium of matter. The assumption of nuclear equilibrium is justified by high temperature. Beta equilibrium is adopted for simplicity: a very rapid cooling of matter at highest temperatures can produce some deviations from beta equilibrium.

Figure 3 shows the composition of matter for $T = 5 \times 10^9$ K , 8×10^9 K, and 1.2×10^{10} K. One can see a temperature dependence for $\rho \lesssim 10^{10}$ g cm^{-3}. On the other hand, for $\rho \gtrsim 10^{12}$ g cm^{-3}, the temperature effects are negligible. If $T \sim 5 \times 10^9$ K, the thermal effects are weak and produce a small admixture of free neutrons at $\rho < \rho_{\rm ND}$. The fraction of free neutrons for $\rho < \rho_{\rm ND}$ rapidly increases with growing temperature, and small fractions of α-particles and free protons appear at $\rho < 10^{10}$ g cm^{-3} ($T = 8 \times 10^9$ K). If $T = 1.2 \times 10^{10}$ K, the nuclei evaporate completely for $\rho \lesssim 10^9$ g cm^{-3}, and the mass fraction contained in free neutrons is significant at any density under discussion. For $\rho \gtrsim 10^{12}$ g cm^{-3}, the temperature effects are negligible.

In contrast to the nuclear composition, the value of Z^2/A depends on temperature rather weakly (Fig. 4). Its density dependence is smooth, because nuclear pairing and shell effects are washed out by temperature.

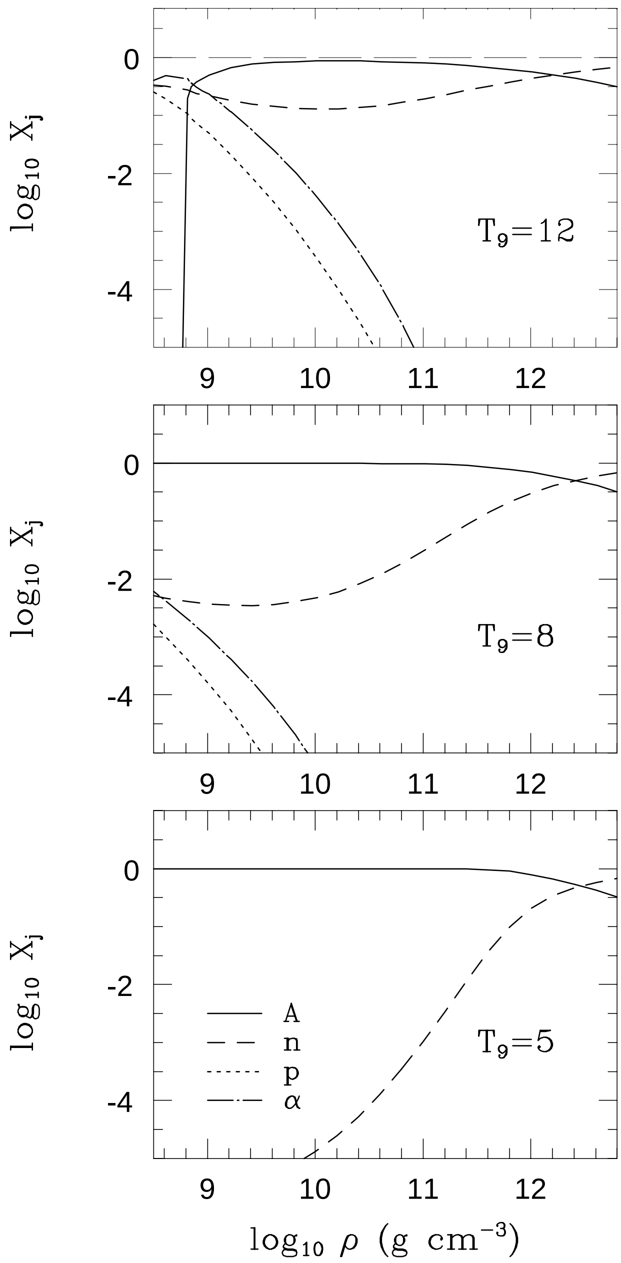

Fig. 3. Mass fractions of various particles versus density at different temperatures $T_9 = T/(10^9$ K) for the model of hot matter, described in the text.

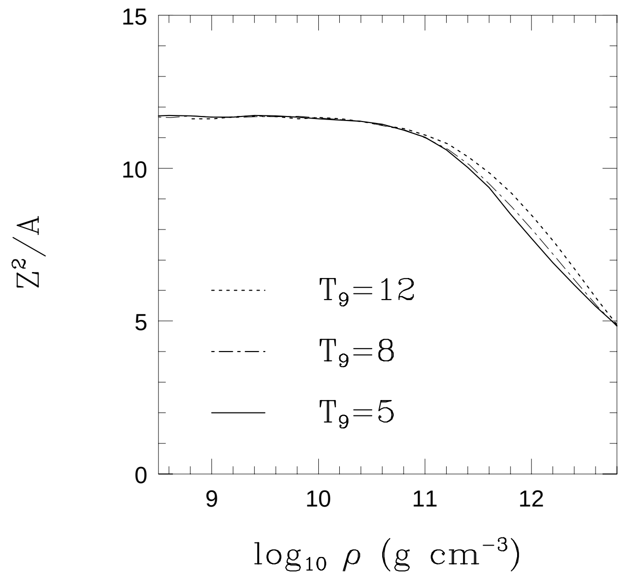

Fig. 4. The nuclear factor Z^2/A, important for NPB, versus matter density ρ, for different temperatures of hot matter.

3. NPB energy loss rate

3.1. General remarks

Let us consider NPB (Eq. (1)) in the case of relativistic degenerate electrons in liquid phase of matter of a neutron star crust ($T > T_{\rm m}$). NPB has been studied by many authors (Sect. 1). Thus we omit the details and outline the derivation of the neutrino energy generation rate in Appendix A.

At the first stage, we adopt the Born approximation and neglect energy exchange between electrons and atomic nuclei. We will discuss the non-Born corrections in Sect. 3.3, and the dynamic effects of nucleus response in Appendix C. We will mostly use the units in which $c = \hbar = k_{\rm B} = 1$.

Let $P = (\varepsilon, \mathbf{p})$ be the electron 4-momentum in the initial state, $P' = (\varepsilon', \mathbf{p}')$ the electron 4-momentum in the final state, and $Q = (\Omega, \mathbf{q})$ be the 4-vector of momentum transfer to a nucleus. Since the energy transfer to a nucleus is neglected we assume Ω=0 throughout Sects. 3 and 4 (although we present general equations in Appendices A and C). Let $K_1 = (\omega_1, \mathbf{k}_1)$ and $K_2 = (\omega_2, \mathbf{k}_2)$ be the 4-momenta of neutrino and antineutrino, respectively, and $K = K_1 + K_2 = (\omega, \mathbf{k})$ be the 4-momentum of the neutrino pair ($\omega = \omega_1 + \omega_2$ and $\mathbf{k} = \mathbf{k}_1 + \mathbf{k}_2$). Energy-momentum conservation implies

$$P = P' + Q + K. \tag{5}$$

As shown in Appendix A, the neutrino energy production rate $Q_{\rm Brem}$ (ergs cm^{-3} s^{-1}) in a relativistic electron gas is

$$\begin{aligned} Q_{\rm Brem} &= \frac{G_F^2 C_+^2\, n_i}{12(2\pi)^{10}} \int {\rm d}\mathbf{k} \int {\rm d}\mathbf{p} \int {\rm d}\mathbf{p}'\, |U(\mathbf{q})|^2 \\ &\times\; f(1-f')\frac{\omega}{\varepsilon\varepsilon'} J_+\,, \end{aligned} \tag{6}$$

where $G_{\rm F} = 1.436 \times 10^{-49}$ ergs cm^3 is the Fermi weak coupling constant, $C_+^2 = C_V^2 + C_A^2 + 2({C'}_V^2 + {C'}_A^2)$ is expressed in terms of vector and axial vector constants (Appendix A) and takes into account generation of electron neutrinos (C_V and C_A; weak neutral + charged currents) and also of muonic and tauonic neutrinos (${C'}_V$ and ${C'}_A$; neutral currents), $U(\mathbf{q})$ is the Fourier transform of the electron-nucleus Coulomb potential, J_+ is the spin averaged squared matrix element in the limit of ultrarelativistic electrons. Furthermore,

$$f = \left[1 + \exp\left(\frac{\varepsilon - \mu}{T}\right)\right]^{-1} \tag{7}$$

is the Fermi-Dirac function for the initial electron, $f' \equiv f(\varepsilon')$ is the same function for the final electron, and μ is the electron chemical potential. Integration in (6) is to be carried out over the domain where $K^2 \geq 0$.

It is convenient to express $Q_{\rm Brem}$ in the form (in the ordinary physical units)

$$\begin{aligned} Q_{\rm Brem} &= \frac{8\pi G_{\rm F}^2 Z^2 e^4 C_+^2}{567 \hbar^9 c^8} (k_{\rm B}T)^6 n_i L \\ &\approx\; 3.229 \times 10^{17}\, \rho_{12}\, X_A\, \frac{Z^2}{A}\, T_9^6 L \;{\rm ergs\ s^{-1}\ cm^{-3}}, \end{aligned} \tag{8}$$

where X_A is the mass fraction contained in nuclei, and ρ_{12} is density in the units of 10^{12} g cm^{-3}. Numerical expression for $Q_{\rm Brem}$ is obtained for the emission of ν_e, ν_μ, ν_τ, $C_+^2 \approx 1.675$, with the Weinberg angle $\sin^2\Theta_W \approx 0.23$ (see Appendix A). In Eq. (8) we have introduced the dimensionless quantity L. We will see (Sects. 3.3 and 3.4) that $L \sim 1$ is a slowly varying function of density, temperature and nucleus parameters which has meaning of a *Coulomb logarithm.* Thus the problem reduces to evaluating L. Note that if we replace $3.23 \times 10^{17}\, L$ by 2.18×10^{17}, then Eq. (8) transforms into the well known formula of Soyeur & Brown (1979).

3.2. Screened Coulomb potential

The squared Fourier transform of the Coulomb potential screened by the plasma polarization (which enters Eq. (6)) can be written as

$$|U(\mathbf{q})|^2 = \frac{(4\pi Z e^2)^2}{q^4 |\epsilon(q)|^2}\, S(q) |F(q)|^2. \tag{9}$$

In this case $F(q)$ is a nuclear formfactor which takes into account the proton charge distribution in a nucleus, $S(q)$ is the static structure factor of ions that describes the ion screening due to ion-ion correlations, and $\epsilon(q)$ is the static longitudinal dielectric function of the electron gas, which accounts for the electron screening.

It is easy to show that the electron screening is always static for the conditions of study. The dielectric function of the degenerate electrons was derived by Jancovici (1962). In the ultrarelativistic limit

$$\epsilon(q) = 1 + \frac{k_{\rm TF}^2}{q^2}\left(\frac{2}{3} + \frac{1-3y^2}{6y}\ln\left|\frac{1+y}{1-y}\right| + \frac{y^2}{3}\ln\left|\frac{y^2}{1-y^2}\right|\right), \tag{10}$$

where

$$y = \frac{q}{2p_{\rm F}}, \qquad k_{\rm TF} = p_{\rm F}\left(\frac{4e^2}{\pi\hbar v_{\rm F}}\right)^{1/2}, \tag{11}$$

$k_{\rm TF}$ being the electron static screening momentum, and $v_{\rm F}$ the electron Fermi velocity. In the long-wavelength limit ($q \ll p_{\rm F}$), one has

$$\epsilon(q) = 1 + \frac{k_{\rm TF}^2}{q^2}, \tag{12}$$

which corresponds to the Debye screening. Actually this approximation appears to be quite satisfactory although we have used exact dielectric function (10) in numerical calculations.

For a spherical nucleus with a uniform proton core,

$$F(q) = \frac{3}{(qr_0)^3}\left[\sin(qr_0) - qr_0\cos(qr_0)\right]. \tag{13}$$

Here r_0 is the core radius which can be smaller than the nucleus radius, for neutron-rich nuclei. One has $F(q) = 1$, for point-like nuclei.

The structure factor $S(q)$ in (9) has been calculated by many authors (e.g., Itoh et al. 1983) for a one-component classical plasma of ions with the uniform electron background. In a strongly coupled plasma ($\Gamma \gtrsim 1$), $S(q)$ cannot be evaluated analytically. Its general feature is that it is greatly suppressed in the long-wavelength limit, $qa \lesssim 1$ (a is defined in Eq. (4)). Thus $S(q)$ produces the screening of the Coulomb interaction with the screening momentum $\sim 1/a$.

Note that actually the structure factor can be influenced by response of neutron gas, which surrounds atomic nuclei in dense matter, to the motion of nuclei. This effect has not been considered so far in the literature. We will use the conventional structure factors (Itoh et al. 1983), assuming that the inclusion of this effect can be reduced to proper choice of the fraction of free neutrons and the number of neutrons bound in nuclei (i.e., proper determination of the nucleus mass number).

The electron and ion screenings suppress the Coulomb interaction for small q while the nuclear formfactor reduces the interaction for large $q \gtrsim 1/r_0$. For typical parameters of dense stellar matter, the ion screening is more efficient than the electron one ($k_{\rm TF} < a^{-1}$).

3.3. Coulomb logarithm

Using Eqs. (6, 8) and (9) we come to the general expression for the Coulomb logarithm (here and below again $\hbar = c = k_{\rm B} = 1$):

$$L = \frac{189}{2^{11}\pi^9 T^6}\int {\rm d}\mathbf{k}\,{\rm d}\mathbf{p}\,{\rm d}\mathbf{p}'\frac{1}{q^4\varepsilon\varepsilon'}\,\frac{S(q)|F(q)|^2}{|\epsilon(q)|^2} \times f(1-f')\,\omega J_+. \tag{14}$$

Let us simplify the integration. Since the electrons are strongly degenerate, the main contribution to L comes from those electron transitions in which the electron momenta $\mathbf{p}$ and $\mathbf{p}'$ lie in the narrow thermal shell around the Fermi surface, $|\varepsilon - \mu| \lesssim T$ and $|\varepsilon' - \mu| \lesssim T$. Let $q_s \sim 1/a$ be the typical screening momentum (Sect. 3.2). We assume that $q_s \ll p_{\rm F}$ to simplify our analysis.

Let $\mathbf{q} = \mathbf{q}_t + \mathbf{q}_r$, where $\mathbf{q}_t$ corresponds to purely elastic Coulomb scattering while $\mathbf{q}_r$ takes into account inelasticity. Here the inelasticity means that the length of electron momentum changes slightly due to the Coulomb interaction although the energy transfer to the nucleus is absent. The process is kinematically allowed since two neutrinos are also involved in energy-momentum conservation. Let us also introduce the vector $\mathbf{p}'' = \mathbf{p} - \mathbf{q}_t = \mathbf{p}' + \mathbf{q}_r + \mathbf{k}$ which is directed along $\mathbf{q}_r$ but has the same length as $\mathbf{p}$.

Note that $q_t = 2p\sin(\theta/2) \approx 2p_{\rm F}\sin(\theta/2)$, where θ is an angle between $\mathbf{p}$ and $\mathbf{p}''$. From geometrical consideration we obtain

$$q^2 = (\mathbf{q}_t + \mathbf{q}_r)^2 = q_t^2 + q_r^2 - q_t^2\left(\frac{q_r}{p_{\rm F}}\right). \tag{15}$$

The neutrino-pair momentum $\mathbf{k}$ can be presented as $\mathbf{k} = \mathbf{k}_t + \mathbf{k}_r$, where $\mathbf{k}_r$ and $\mathbf{k}_t$ are the orthogonal vector components parallel and perpendicular to $\mathbf{p}''$, respectively. Strong electron degeneracy implies that q_r and k are much smaller than $p_{\rm F}$ although q_t can be comparable with $p_{\rm F}$ for large-angle electron scattering events. Therefore, NPB is accompanied by nearly elastic Coulomb scattering. Then the neutrino-pair energy is

$$\omega = \frac{\varepsilon^2 - \varepsilon'^2}{\varepsilon + \varepsilon'} \approx k_r + q_r. \tag{16}$$

The condition $K^2 = \omega^2 - \mathbf{k}^2 \approx k_0^2 - k_t^2 > 0$ requires $k_0 \geq k_t$, where $k_0^2 = q_r(2\omega - q_r)$, or $q_r > 0$, $\omega > q_r/2$. Furthermore, we set ${\rm d}\mathbf{p} = {\rm d}\Omega\varepsilon^2{\rm d}\varepsilon$, where ${\rm d}\Omega$ is solid angle element in the direction of vector $\mathbf{p}$. The integration over ε under strong electron degeneracy is standard:

$$\int {\rm d}\varepsilon f(1-f') = \frac{\omega}{{\rm e}^{\omega/T} - 1}. \tag{17}$$

The integration over $\mathbf{p}'$ can be replaced by the integration over $\mathbf{q}$, with ${\rm d}\mathbf{q} = 2\pi q_t\,{\rm d}q_t\,{\rm d}q_r$. Note also, that ${\rm d}k_r = {\rm d}\omega$.

This yields

$$L = \frac{189}{2^{11}\pi^9 T^6}\, 8\pi^2 \int_0^\infty \mathrm{d}q_r \int \mathrm{d}q_t \; q_t \, \frac{S(q)|F(q)|^2}{q^4|\epsilon(q)|^2} \times \int_{q_r/2}^\infty \mathrm{d}\omega \, \frac{\omega^2}{\mathrm{e}^{\omega/T}-1} \int_0^{k_0} \mathrm{d}k_t \; k_t \int_0^{2\pi} \mathrm{d}\varphi \; J_+, \tag{18}$$

where φ is an azimuthal angle of $\mathbf{k}$ with the polar axis along $\mathbf{p}''$. The expression for J_+ is given by Eq. (A14) in Appendix A. Using this expression and the relation $\mathbf{q}_t\mathbf{k} = -2p_\mathrm{F} k_r \sin^2(\theta/2) + p_\mathrm{F} k_t \sin\theta \cos\varphi$, we can integrate over φ and k_t and present L in the form

$$L = \frac{1}{T} \int_0^{2p_\mathrm{F}} \mathrm{d}q_t \; q_t^3 \int_0^\infty \mathrm{d}q_r \; \frac{S(q)|F(q)|^2}{q^4|\epsilon(q)|^2} \times R_T(y,u)\, R_\mathrm{NB}(q_t), \tag{19}$$

where $y = q_t/(2p_\mathrm{F}) = \sin(\theta/2)$, $u = q_r/T$, and q is given by (15). Here we introduce the factor R_NB to take into account deviations from the Born approximation (see below). The integration over q_r describes the *thermal effects*, i.e., a weak inelasticity in Coulomb scattering due to a finite width of the thermal shell around the electron Fermi surface. In Eq. (19) these effects are controlled by the function

$$\begin{aligned} R_T(y,u) &= \frac{189}{16\pi^6} \left\{ \int_{u/2}^{u/(2y^2)} \mathrm{d}v \frac{v^2}{\mathrm{e}^v - 1} \left(v - \frac{u}{2}\right)^2 \right. \\ &\times \left[1 - \frac{2}{3u}\, \frac{y^2}{1-y^2} \left(v - \frac{u}{2}\right)\right] \\ &+ \frac{u}{2}\, \frac{1-y^2}{y^2} \int_{u/(2y^2)}^\infty \mathrm{d}v \; \frac{v^2}{\mathrm{e}^v - 1} \\ &\times \left. \left[v - \frac{u}{2} - \frac{u}{6}\, \frac{1-y^2}{y^2}\right] \right\}, \end{aligned} \tag{20}$$

where $v = \omega/T$. The thermal effects introduce an additional screening of the Coulomb interaction with the screening momentum $\sim T$. The properties of $R_T(y,u)$ are analyzed in Appendix B, where we present also a convenient fitting expression for this function.

Finally, let us discuss the non-Born correction R_NB in (19). Since dense stellar matter contains heavy nuclei (Sect. 2), the Born approximation used in all previous works is not very accurate. Exact calculation of the NPB rate beyond the Born approximation is difficult but we propose an approximate treatment of the non-Born terms, which is explained below.

A process of NPB consists of two stages: electron scattering on a nucleus, and neutrino-pair emission. As seen from the above results the electron scattering is much stronger (i.e., it is accompanied by larger momentum transfers) than the neutrino-pair emission except possibly for the small-angle scattering. However one cannot expect large deviations from the Born approximation for small-angle scattering (Berestetskii et al. 1982). Thus we can use the well known method of soft photons (Berestetskii et al. 1982) and claim that the NPB rate is proportional to the product of the cross section of the elastic electron - nucleus scattering and the probability of the neutrino-pair emission. The pair emission involves weak interaction and cannot be affected strongly by the Born approximation. Hence the main impact of the Born approximation is on the elastic scattering cross section. We expect that the non-Born correction factor is $R_\mathrm{NB}(q_t) = \sigma(q_t)/\sigma_\mathrm{Born}(q_t)$, where $\sigma(q_t)$ is the exact elastic cross section with the momentum transfer q_t, and $\sigma_\mathrm{Born}(q_t)$ is the Born cross section. The factor $R_\mathrm{NB}(q_t)$ has been calculated by many authors (e.g., Doggett & Spencer, 1956), and its inclusion into the Coulomb logarithm is straightforward.

3.4. Low- and moderate-temperature cases

We have reduced the problem of calculating the Coulomb logarithm to a two dimensional integration in (19). One can distinguish two cases: *the low-temperature case* when temperature is lower than the Coulomb screening momentum, $T \ll q_s$, and *the moderate-temperature case* when $q_s \lesssim T \ll T_\mathrm{F}$.

All previous studies of NPB from the relativistic degenerate electrons have used the approximations appropriate to *the low-temperature case*. In this case the main contribution into L comes from the values of $q_t \gg T$. Then R_T is a sharp function of q_r which decreases rapidly with increasing $q_r \gtrsim T$ (Appendix B). Therefore, we can set $q_r = 0$ in the remaining functions under the integral (19), and the integration over q_r is performed with the aid of Eq. (B1):

$$L = \int_0^{2p_F} q^3 \; \mathrm{d}q \, \frac{S(q)|F(q)|^2}{q^4|\epsilon(q)|^2} \, R_c(y)\, R_\mathrm{NB}(q) \; , \tag{21}$$

where $q = q_t$, $y = q/(2p_\mathrm{F})$ and

$$R_c(y) = 1 + \frac{2y^2}{1-y^2} \ln(y). \tag{22}$$

Equations (8) and (21) with $R_\mathrm{NB} = 1$ reproduce the familiar NPB rate for degenerate and relativistic electrons. For example, these equations can be obtained from the results of Itoh & Kohyama (1983), taking into account that

$$\int_0^1 \mathrm{d}x \, \frac{x(1-x^2)}{y\xi} \ln\left|\frac{yx+\xi}{yx-\xi}\right| = \frac{2}{3}\, R_c(y)\, \frac{1}{1-y^2}, \tag{23}$$

where $\xi = \sqrt{1 - x^2(1-y^2)}$. The quantity F_liquid introduced by Itoh & Kohyama (1983) is equal to $(2/3)L$, and their function $I_2(q) = (8/3)\, y^2\, R_c(y)$.

We see that L has, indeed, the meaning of *the Coulomb logarithm.* If the screening of the Coulomb potential were weak ($S(q) = \epsilon(q) = 1$) and $R_c \approx 1$ (which is true for $q \ll p_\mathrm{F}$), then L would acquire a familiar logarithmic divergency at small q. The divergency is eliminated due to the screening functions (Sect. 3.2). The function R_c, Eq. (22), introduces additional screening which comes from the squared matrix element of the NPB reaction. We have $R_c \to 1$ for small-angle scattering ($y \to 0$), while $R_c \approx (1-y^2)/2 \to 0$ for backscattering ($y \to 1$). Therefore R_c suppresses the backscattering (just as $F(q)$) which is natural for relativistic electrons (Berestetskii et al. 1982).

The *low-temperature* Coulomb logarithm L is expressed as a simple one dimensional integral (21), which is easily computed (Sect. 3.5) for any parameters of dense stellar matter.

In the *moderate-temperature* case ($q_s \lesssim T \ll T_\mathrm{F}$), one should deal with two dimensional integration (19) which is also easy once the thermal function $R_T(y,u)$ is known (Appendix B).

3.5. Numerical results

In the degenerate electron gas and Coulomb liquid of atomic nuclei, the Coulomb logarithm depends actually on four parameters: on nuclear charge number Z that defines the ion screening (Sect. 3.2), on the proton core nuclear radius r_0 (see (13)), on density ρ and T. The ion coupling parameter Γ, Eq. (4), is expressed through Z, ρ and T. In the ultra-relativistic limit ($x \gg 1$) the four parameters can be replaced by three dimensionless parameters

$$L = L(Z,\eta,t), \quad \eta = \frac{r_0}{a}, \quad t = \frac{k_\mathrm{B} T}{2 p_\mathrm{F} c} \approx \frac{T}{2 T_\mathrm{F}}, \qquad (24)$$

where a is the ion-sphere radius (see Eq. (4)), and T_F is given by Eq. (3).

We have calculated L from Eq. (19) for $Z = 10$, 20, 30, 40, 50, and for wide ranges of $\eta \lesssim 0.2$ and $t \lesssim 0.1$ in the Coulomb liquid ($T > T_m$, i.e., $t > 1.1 \times 10^{-5} Z^{5/3}$, Sect. 2.1). The structure factor $S(q)$ has been taken from Itoh et al. (1983). Typical results are presented in Figs. 5 and 6.

At small t, our values of L tend to those obtained in the low-temperature approximation (cf., curves 3 and 4 in Figs. 5 and 6). At higher t, the deviations from the latter approximation are quite pronounced. In the low-temperature approximation, L depends on T only through the structure factor $S(q)$ (which slightly varies with Γ), and L grows slowly with t due to weakening of the ion screening. An inclusion of the thermal effects (Sects. 3.3 and 3.4) leads to a stronger and non-monotonic temperature dependence of L which can be explained as follows. The thermal effects are described by the function R_T which, generally, introduces an additional 'thermal screening' of the Coulomb interaction and tends to suppress L and the NPB rate. However the thermal effects act within the thermal shell near the electron Fermi surface. Deviations of the electron momenta from the Fermi sphere can decrease the momentum transfers q, Eq. (15), for a given q_t. Since the NPB rate, Eqs. (8), (19), involves q^{-4} (squared Coulomb potential), the decrease of q causes a noticeable growth of L with t at low t (Figs. 5 and 6). With increasing t, the 'thermal screening' itself becomes more important and suppresses L at higher t.

Figures 5 and 6 also show variation of the Coulomb logarithm with Z. The Coulomb logarithm increases with Z which is evidently the effect of the ion screening ($q_s/p_\mathrm{F} \sim Z^{-1/3}$): the smaller the ratio q_s/p_F, the larger the reaction rate. Similar effects in the low-temperature case are well known (e.g., Itoh & Kohyama 1983).

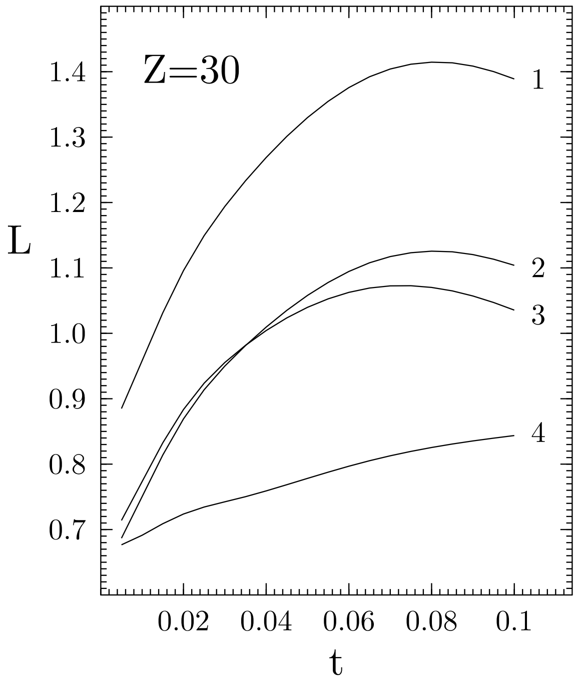

Fig. 5. The NPB Coulomb logarithm L vs. dimensionless temperature t (24) for $Z = 30$ nuclei. Curve 1 – point-like nuclei ($\eta = r_c/a = 0$); 2 – finite-size nuclei with $\eta = 0.2$; 3 – same as 1 but in the Born approximation; 4 – point-like nuclei, non-Born corrections and thermal effects are neglected ('standard approach' of previous works).

The calculations show that finite size of nuclei (nuclear formfactor) becomes significant for $\eta \gtrsim (0.1 - 0.2)$. With increasing η, the Coulomb logarithm noticeably decreases since the nuclear formfactor introduces an effective screening of the Coulomb interaction (Sect. 3.2). Finite-size effects are negligible in the outer crust of a neutron star, where $\eta \ll 1$, but they are strong in the inner crust, where the atomic nuclei occupy a substantial fraction of volume.

Finally, let us emphasize the importance of the non-Born corrections. According to Doggett & Spencer (1956), the non-Born correction factor R_NB increases the electron

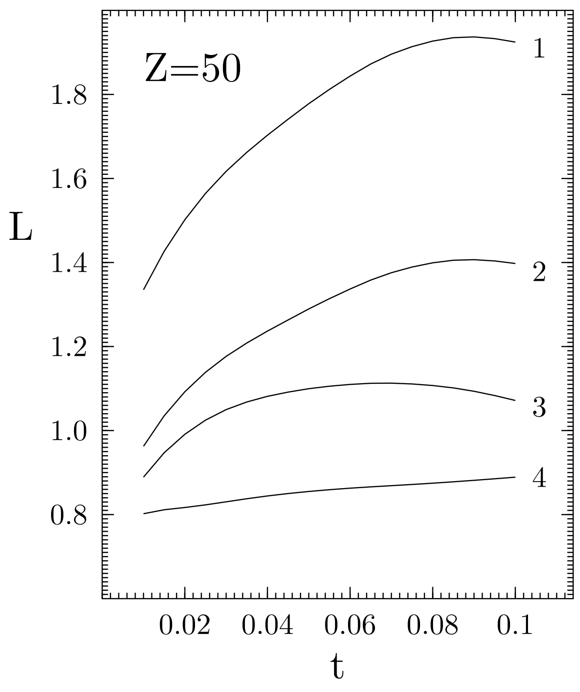

Fig. 6. Same as in Fig. 5, but for Z=50.

- nucleus scattering cross section, $R_{\rm NB} > 1$, and the increase is larger for higher Z. Accordingly, an inclusion of this factor amplifies quite noticeably the Coulomb logarithm as seen from Figs. 5 and 6. For $Z \gtrsim 30$, this effect is even more important than the thermal effect described above.

Comparing our improved values of L which include the thermal and non-Born corrections (curves 1 in Figs. 5 and 6) with the non-corrected values (curves 4), relevant to the "traditional" results, we conclude that our corrections amplify L and the NPB rate, typically, by a factor of 1.5 – 2.5.

For a practical use, we can propose an analytic fit:

$$\begin{aligned} L &= A/B^{3/4}, \qquad (25) \\ A &= 0.269 + 20t + 0.0168Z + 0.00121\eta - 0.0356Z\eta \\ &+ 0.0137Z^2t + 1.54Zt\eta, \\ B &= 1 + 180t^2 + 0.483tZ + 20tZ\eta^2 + 4.31 \times 10^{-5}Z^2. \end{aligned}$$

This formula reproduces all calculated values of L ($Z \leq 50$, $t \lesssim 0.1$, $\eta \lesssim 0.2$) with the mean error of about 1%, and with the maximum error of 2.3% at $Z = 10$, $t = 0.001$ and $\eta = 0.2$.

Thus the NPB energy loss rate $Q_{\rm Brem}$ can be easily calculated from Eqs. (8) and (25) for any model of dense matter (provided the values of ρ, T, n_e, Z, A, X_A, and r_0 are specified). If matter consists of nuclei of various species (A, Z), one should sum over the species in Eq. (8). Actually, NPB from a multi-component mixture of nuclei deserves a separate study. We expect, however, that our results (obtained for one component plasma of nuclei) can be used, at least semi-quantitatively, for the mixtures as well.

Note that Cazzola et al. (1971) and Munakata et al. (1987) considered the NPB of non-degenerate and weakly degenerate electrons. In this case the thermal shell washes out the Fermi surface, and the thermal effects are naturally implanted in the equations. However the above authors analyzed ideal plasma of ions $\Gamma \ll 1$ (neglecting the ion screening) and weak degeneracy ($T/T_{\rm F} \gtrsim 0.3$) – the conditions which are not relevant for applications and opposite to those studied in our work.

Figure 7 shows the density dependence of the NPB energy loss rate $E_{\rm Brem} = Q_{\rm Brem}/\rho$ (logarithmic scale) for three models of dense matter (Sect. 2) at several T. For the ground state and accreted matter, the NPB is produced by electron scattering on nuclei (A, Z) of one species (Sect. 2). In the case of the hot matter, we take into account the contribution of nuclei, protons and α particles. Note that self-consistent models of accreted matter correspond to $T \gtrsim 10^8$ K (e.g., Miralda-Escudé et al. 1990). We use such a model at higher T for illustrative purpose, to show how possible scatter in nuclear composition affects the NPB rate. The rates for accreted and ground state matters are shown at $T \leq 5 \times 10^9$ K, while the rate in the hot matter is displayed at $T \geq 5 \times 10^9$ K (Sect. 2). If $T \sim 5 \times 10^9$ K, all three models are possibly not very accurate. We present three curves at $T = 5 \times 10^9$ K to visualize the effects of nuclear composition. The NPB rates at this temperature are shown separately in Fig. 8 in natural scale. It is seen that they differ by a factor of 2 – 4.

At $T = 10^9$ K and 2×10^9 K, in the considered density region $10^8 - 10^{13}$ g cm $^{-3}$ the matter may be in liquid and crystal phases. The quantity $E_{\rm Brem}$ in the crystal phase was calculated using simple approximations obtained recently by two of the authors (Yakovlev & Kaminker 1996) for neutrino pair emission due to the electron-phonon scattering. The ground state matter is crystallized for $\rho > 2.35 \times 10^{10}$ g cm $^{-3}$ at $T = 10^9$ K (not for all densities, see below) and for $\rho > 1.3 \times 10^{11}$ g cm $^{-3}$ at $T = 2 \times 10^9$ K. The accreted matter is crystallized for $\rho > 2.14 \times 10^{11}$ g cm $^{-3}$ (not for all densities) only at $T = 10^9$ K. The melting temperature for the accreted matter is smaller (Fig. 2) due to lower values of Z, and the crystallization occurs at higher ρ (if T is fixed). It should be noticed that there are two types of jumps of the NPB rate for the ground state and accreted models. The jumps of the first type result from the jumps of Z and A (Sect. 2, Figs. 1, 2). Such jumps take place at $T = 10^9$ K, 2×10^9 K and 5×10^9 K (Figs. 7, 8). The other more pronounced jumps come from transitions from liquid phase to crystal and back at some densities. One may see single 'back' transition from crystal to liquid for the ground state matter and a few ones for the accreted matter at $T = 10^9$ K (Fig. 7). The 'back' transitions come from nonmonotonic character of melting temperature due to the jumps of Z (see Fig. 2). When T is fixed and $\rho \gtrsim 3 \times 10^9$ g cm^{-3}, the NPB rate for the ground state matter in the liquid phase is, generally, several times higher than for the accreted matter due to larger values of Z (Sect. 2).

Note, however, the striking general similarity of the NPB rates in the liquid and solid phases (Fig. 7). It results from the similarity of the expressions for the NPB rates (cf. Eq. (21) with Eqs. (13) and (14) of Yakovlev & Kaminker 1996) and reflects common properties of strongly coupled Coulomb liquid and high-temperature Coulomb crystal.

The NPB rate in the hot matter for $T = 1.2 \times 10^{10}$ K (Fig. 7) is broken at densities $\rho \lesssim 2 \times 10^8$ g cm^{-3} at which the electron degeneracy becomes low and our results are invalid. Note a sharp drop of the NPB rate at $\rho \lesssim 10^9$ g cm^{-3} for this T. It occurs due to dissociation of nuclei (Fig. 3): the contribution of nuclei into the NPB becomes negligible but a smaller contribution of protons and α-particles is available. The drop clearly indicates the importance of coherence effect ($Q_{\rm Brem} \propto Z^2$) which amplifies significantly the NBP rate in the presence of high-Z nuclei. For other T and ρ, the contribution of protons and α-particles is insignificant.

If Z, A, X_A, and L were independent of density, the NPB rate $E_{\rm Brem} = Q_{\rm Brem}/\rho$ would also be density independent (at fixed T). However, as seen from Figs. 7 and 8, the NPB energy loss rate $E_{\rm Brem}$ decreases mainly with ρ at $\rho \gtrsim 10^{10}$ g cm^{-3}. This decrease is explained mostly by the lowering of Z^2/A, (Figs. 1 and 4), fraction of nuclei X_A, and of the Coulomb logarithm L.

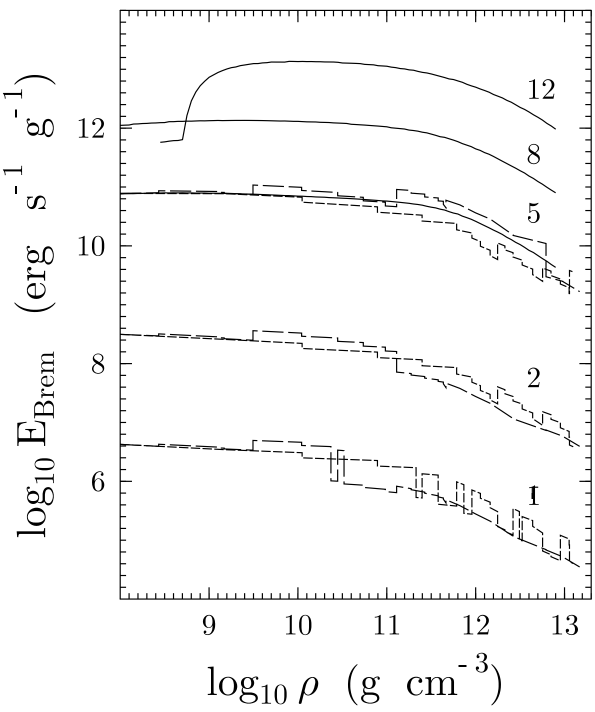

Fig. 7. The NPB energy loss rate $E_{\rm Brem} = Q_{\rm Brem}/\rho$ (in erg g^{-1} s^{-1}, logarithmic scale) vs. density (in g cm^{-3}) for T_9=1, 2, 5, 8, 12 (figures near curves). Solid line – hot matter; long dashes – ground state matter, short dashes – accreted matter.

4. Conclusions

We have analyzed nuclear composition of neutron star crusts (Sect. 2) for three models of dense matter: cold catalyzed matter, accreted matter, and hot matter in thermodynamic equilibrium. The first and second models are valid for $T \lesssim 5 \times 10^9$ K, while the third one is appropriate for higher temperatures. Nuclear composition (A, Z), melting temperature and other properties of dense matter are different for these models.

In Sect. 3 we have reconsidered the neutrino-pair bremsstrahlung (1) of relativistic degenerate electrons due to scattering on atomic nuclei at $T > T_{\rm m}$. We have shown that the neutrino energy generation rate can be expressed (Eq. (8)) through a Coulomb logarithm L, which varies slowly in stellar matter. We have obtained a general expression (19) for L, which takes into account two effects neglected in previous works. First, it includes the non-Born corrections, and, second, it describes the thermal effects associated with the finite width of the shell around the electron Fermi surface. The thermal effects are shown to be quite important at moderate electron degeneracy, and they lead to the appearance of the new 'moderate temperature regime' (Sect. 3.4) overlooked in previous studies of NPB from relativistic degenerate electrons. We have calculated the Coulomb logarithm numerically for possible parameters of dense matter in neutron star crusts, and found a simple analytic fit (25).

Note that NPB of electrons in a Coulomb liquid of atomic nuclei is similar to NPB at $T < T_m$ produced due to Coulomb scattering of electrons on 'charged impurities' – nuclei $(A_{\rm imp}, Z_{\rm imp})$ immersed accidentally in a lattice of bulk nuclei (A, Z). When the nuclei crystallize ($T < T_{\rm m}$) but temperature does not drop much below $T_{\rm m}$, the most important is the neutrino pair generation due to electron phonon scattering in solid matter (this follows from the recent results of Pethick & Thorsson 1994). The neutrino energy generation rate drops rapidly with decreasing T at $T \ll T_{\rm m}$ (e.g., Itoh et al. 1984b, Yakovlev & Kaminker 1996), and the Coulomb impurity scattering can be dominant even for not very low T. The energy generation rate $Q_{\rm imp}$ is obviously given by the expression similar to (8) but with $n_{\rm i}$ replaced by the impurity number density $n_{\rm imp}$, and with Z^2 replaced by $(Z_{\rm imp} - Z)^2$. The expression for $Q_{\rm imp}$ contains a Coulomb logarithm $L_{\rm imp}$ which should be quite similar to the Coulomb logarithm (21) in liquid matter

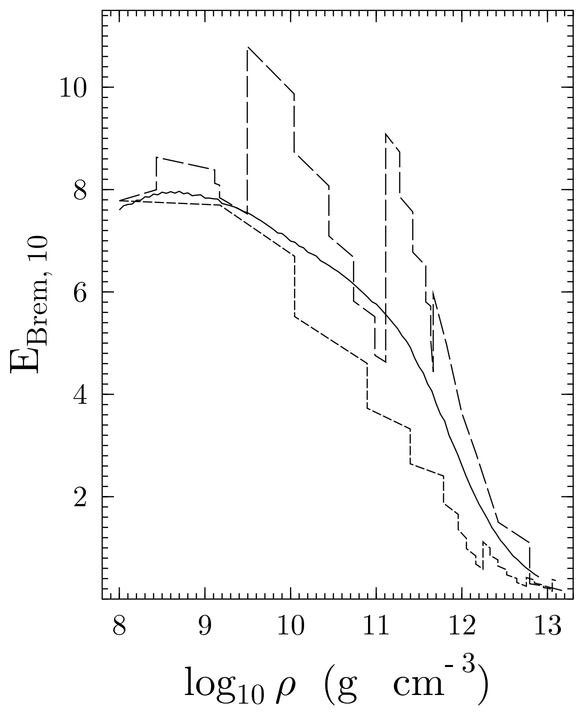

Fig. 8. Same as in Fig. 7, but for $T = 5 \times 10^9$ K (linear scale). The plotted quantity is $E_{\rm Brem,10}$ (the loss rate $E_{\rm Brem}$ in units of 10^{10} ergs s^{-1} g^{-1}).

(although the thermal effects become unimportant). The major difference is in the Coulomb screening. In solid matter, the screening is described by the impurity structure factor $S_{\rm imp}(q)$ which takes into account impurity distribution over lattice sites. If the impurity correlation length is large, the main contribution into the screening comes from the electrons.

The results of the present article can be useful for numerical modeling various phenomena related to the thermal evolution of neutron stars. First of all, we should mention cooling of young neutron stars (of age $t \lesssim (1 - 10^3)$ yrs) where internal thermal relaxation is not achieved (Lattimer et al. 1994). The thermal relaxation is accompanied by the propagation of the cooling wave from the interior to the surface. The associated variations of surface temperature are, in principle, observable. The dynamics of thermal relaxation is sensitive to the properties of matter in the neutron star crust, particularly to nuclear composition and neutrino generation mechanisms. In addition, the above results are useful for studying thermal evolution of accreting neutron stars (see, e.g., Miralda-Escudé et al. 1990, and references therein).

Acknowledgements. This work was supported partly by INTAS, grant No. 94-3834, the Russian Basic Research Foundation, grant No. 96-02-16870a, and by the ESO C&EE Programme, grant No. A-01-068. We acknowledge also the support of the Polish State Committee for Scientific Research (KBN), grant No. 2 P304 014 07.

Appendix A: NPB matrix elements and energy loss rate

Using the notations introduced in Sect. 3.1, the NPB energy loss rate in the Born approximation can be generally written as ($\hbar = k_{\rm B} = c = 1$):

$$Q_{\rm Brem} = \frac{n_i}{(2\pi)^{11}} \int {\rm d}\mathbf{p} \int {\rm d}\mathbf{p}' \int {\rm d}\mathbf{k}_\nu \int {\rm d}\mathbf{k}'_\nu \times \delta(\varepsilon - \varepsilon' - \omega)\omega f(1-f')W, \tag{A1}$$

where

$$W = \frac{G_F^2}{2} \, \frac{1}{(2\omega_\nu)(2\omega'_\nu)(2\varepsilon)(2\varepsilon')} \sum_{\sigma,\nu} |M|^2, \tag{A2}$$

$|M|^2$ is the squared matrix element. Summation is over the electron spin states σ before and after scattering and over neutrino flavors (ν_e, ν_μ, ν_τ). When the neutrino energies are much lower than the intermediate boson mass ($\sim$80 GeV) the standard approach yields

$$\begin{aligned} \sum_\sigma |M|^2 &= \int {\rm d}\mathbf{q}\, |U(\mathbf{q})|^2 \, \delta(\mathbf{p} - \mathbf{q} - \mathbf{p}' - \mathbf{k}) \\ &\times \ {\rm Tr}(\hat{K}_1 O^\alpha \hat{K}_2 O^\beta) \\ &\times \ {\rm Tr}\left[(\hat{P}' + m) L_\alpha (\hat{P} + m) \bar{L}_\beta\right], \end{aligned} \tag{A3}$$

$$O^\alpha = \gamma^\alpha (1 + \gamma^5),$$

$$L_\alpha = \Gamma_\alpha G(P - Q)\gamma^0 + \gamma^0 G(P' + Q)\Gamma_\alpha, \tag{A4}$$

$$G(P) = \frac{\hat{P} + m}{P^2 - m^2}, \qquad \Gamma^\alpha = C_V \gamma^\alpha + C_A \gamma^\alpha \gamma^5. \tag{A5}$$

Here $U(\mathbf{q})$ is the Fourier transform of the Coulomb potential (Sect. 3.2), m is the electron mass, $G(P)$ is the free-electron propagator, γ^α is a Dirac matrix, upper bar denotes Dirac conjugate, and $\hat{P} = P_\alpha \gamma^\alpha$ (Berestetskii et al. 1982). Furthermore, C_V and C_A are, respectively, the vector and axial vector weak interaction constants. For the emission of electron neutrino (charged + neutral currents), one has $C_V = 2\sin^2\theta_W + 0.5$ and $C_A = 0.5$, while for the emission of muonic or tauonic neutrinos (neutral currents only), $C'_V = 2\sin^2\theta_W - 0.5$ and $C'_A = -0.5$. Here θ_W is the Weinberg angle, $\sin^2\theta_W \simeq 0.23$.

Using the well known identity

$$\int {\rm d}\mathbf{k}_\nu \int {\rm d}\mathbf{k}'_\nu \, \delta^{(4)}(K - K_1 - K_2) \, \frac{K_1^\alpha K_2^\beta}{\omega_\nu \omega'_\nu} = \frac{\pi}{6}(K^2 g^{\alpha\beta} + 2K^\alpha K^\beta), \tag{A6}$$

we obtain

$$Q_{\rm Brem} = \frac{G_F^2 \, n_i}{12(2\pi)^{10}} \int {\rm d}\mathbf{k} \int {\rm d}\mathbf{p} \int {\rm d}\mathbf{p}' \, |U(\mathbf{q})|^2 \times f(1-f') \frac{\omega}{\varepsilon\varepsilon'} J, \tag{A7}$$

$$J = \sum_\nu (K^\alpha K^\beta - K^2 g^{\alpha\beta}) \times {\rm Tr}\left[(\hat{P}' + m) L_\alpha (\hat{P} + m) \bar{L}_\beta\right]. \tag{A8}$$

The integration in (A7) is to be carried out over the domain where $K^2 \geq 0$; $g^{\alpha\beta}$ is the metric tensor.

Let us introduce the notations

$$\begin{aligned} u &= (P'+K)^2 - m^2 = 2P'K + K^2, \\ v &= -(P-K)^2 + m^2 = 2PK - K^2. \end{aligned} \tag{A9}$$

Tedious but straightforward calculations yield:

$$\begin{aligned} J &= C_+^2 J_+ + C_-^2 J_-, \\ C_+^2 &= \sum_\nu (C_V^2 + C_A^2), \\ C_-^2 &= \sum_\nu (C_V^2 - C_A^2), \end{aligned} \tag{A10}$$

where

$$\begin{aligned} J_+ &= 8m^2 - 4(m^2+K^2)\left(\frac{u}{v}+\frac{v}{u}\right) \\ &+ \left(\frac{4}{v}-\frac{4}{u}\right)\left[K^2\left(4PP' - 8\varepsilon\varepsilon' + m^2\right.\right. \\ &+ \left.\left. K^2 - 4\omega(\varepsilon-\varepsilon')\right) - 4m^2\omega^2\right] \\ &+ \frac{4}{u^2}K^2(m^2-K^2)(4\varepsilon\varepsilon' - 2PP' \\ &+ 2m^2 + 4\varepsilon\omega - K^2) \\ &+ \frac{4}{v^2}K^2(m^2-K^2)(4\varepsilon\varepsilon' - 2PP' \\ &+ 2m^2 - 4\varepsilon'\omega - K^2) \\ &+ 4K^2(m^2-K^2)\left(\frac{u}{v^2}-\frac{v}{u^2}\right) \\ &+ \frac{8}{uv}\left[4K^2(PP'-m^2)(2\varepsilon\varepsilon' - PP' - m^2)\right. \\ &- 2m^2K^2(2\varepsilon\varepsilon' - PP' + m^2) \\ &+ 4\omega^2(m^2+K^2)PP' - 2m^2\omega^2(2m^2+K^2) \\ &+ \left. K^4(3\varepsilon^2 + 3\varepsilon'^2 + 2\varepsilon\varepsilon' - 2PP' - m^2 - \omega^2)\right] \end{aligned} \tag{A11}$$

and

$$\begin{aligned} J_- &= -8m^2 + 4m^2\left(\frac{u}{v}+\frac{v}{u}\right) \\ &+ \left(\frac{4}{v}-\frac{4}{u}\right)(4\omega^2+K^2) \\ &- \frac{12}{u^2}m^2K^2(4\varepsilon\varepsilon' - 2PP' \\ &+ 2m^2 + 4\varepsilon\omega - K^2) \\ &- \frac{12}{v^2}m^2K^2(4\varepsilon\varepsilon' - 2PP' \\ &+ 2m^2 - 4\varepsilon'\omega - K^2) \\ &- 12m^2K^2\left(\frac{u}{v^2}-\frac{v}{u^2}\right) \\ &+ \frac{8m^2}{uv}\left[K^2(12\varepsilon\varepsilon' + 2PP' - 2m^2 + K^2)\right. \\ &- \left. 2\omega^2(2PP' - 2m^2 + K^2)\right]. \end{aligned} \tag{A12}$$

Equations (A7), (A8) (A11) and (A12) determine the NPB rate for any degree of electron degeneracy and relativism. The equations yield the solution of the problem in a compact and convenient form which allows one to consider easily different limiting cases. In a hot, non-degenerate plasma, where a significant number of positrons can be present in addition to the electrons, the contribution from positrons should be added to $Q_{\rm Brem}$ in the straightforward manner.

Analyzing Eqs. (A11) and (A12) one can show that the main contribution into NPB of relativistic and degenerate electrons comes from J_+. Accordingly, we keep only this term in Eq. (8).

In our case, the neutrino-pair momentum is thermal, $k \lesssim T \ll p_{\rm F}$ but the elastic electron - nucleus momentum transfer can be much larger, $q_t \sim p_{\rm F}$. First consider the case when $q \gg T$ or $q \gg k$. Then we can put $\mathbf{q} \approx \mathbf{p} - \mathbf{p}'$, and the Coulomb scattering is, to a very good approximation, elastic. A careful analysis of various terms in (A11) shows that the main contribution comes from the term

$$\begin{aligned} J_+ &= \frac{8K^2(PP')[2\varepsilon\varepsilon' - (PP')]}{(P'K)(PK)} \\ &= \frac{8(\omega^2 - \mathbf{k}^2)[(\varepsilon\varepsilon')^2 - (\mathbf{pp}')^2]}{(\varepsilon'\omega - \mathbf{p}'\mathbf{k})(\varepsilon\omega - \mathbf{pk})}. \end{aligned} \tag{A13}$$

Here we have adopted the natural approximation: $u = 2P'K$, $v = 2PK$. In addition, we can set $\varepsilon = \varepsilon' = \mu$, $p = p' = p_{\rm F}$ and $(\mathbf{qp})/p = q^2/2p$ (see Sect. 3.3), in smooth functions of electron energy and momentum. One can easily show that $(\varepsilon\varepsilon')^2 - (\mathbf{pp}')^2 \approx p^2\, q^2\, [1 - q^2/(2p^2)]$, $u \approx 2pq_r$ and $v \approx 2p(q_r - (\mathbf{q}_t\mathbf{k})/p)$, where we use the notations of Sect. 3.3. Finally, for the case of $T \ll q$ we obtain

$$J_+ = 8\frac{q_t^2}{q_r}(\omega^2 - k^2)\left(1 - \frac{q_t^2}{4p^2}\right)\left(q_r - \frac{\mathbf{k}\mathbf{q}_t}{p}\right)^{-1}. \tag{A14}$$

Now consider J_+ in the approximation of small-angle scattering ($q \ll p_{\rm F}$). Then k can be comparable to q, and more terms should be kept in J_+. An analysis of Eq. (A11) shows that we must retain the terms

$$\begin{aligned} J_+ &= \frac{32\,K^2}{uv}[(\varepsilon\varepsilon')^2 - (\mathbf{pp}')^2] - 4K^2\left(\frac{v}{u}+\frac{u}{v}\right) \\ &+ 16K^2\left(\frac{1}{u}-\frac{1}{v}\right)(\varepsilon\varepsilon' + \mathbf{pp}') \\ &- 8\,K^4(\varepsilon\varepsilon' + \mathbf{pp}')\left(\frac{1}{u^2}+\frac{1}{v^2}\right) \\ &+ \frac{16K^4}{uv}(\varepsilon+\varepsilon')^2. \end{aligned} \tag{A15}$$

Using energy-momentum conservation and the inequalities $k \ll p$ and $q \ll p$ and introducing the notations of Sect. 3.3, we obtain

$$\begin{aligned} \omega &\approx q_r + k_r, \\ u &\approx v \approx 2pq_r, \\ K^2 &= \omega^2 - k_r^2 - k_t^2 \approx k_0^2 - k_t^2, \\ J_+ &= 8(\omega^2 - k^2)\frac{q_t^2}{q_r^2}. \end{aligned} \tag{A16}$$

Let us compare Eqs. (A14) and (A16) for J_+ obtained, respectively, in the domains of large and small q. Since both domains overlap, we can describe J_+ accurately for all q. However, we see that Eq. (A14) coincides formally with (A16) in the domain of small q, where the terms $q_t^2/(4p^2)$ and $\mathbf{k}\mathbf{q}_t/p$ are negligible second-order corrections. Thus we use Eq. (A14) for all q in Sect. 3.3.

Appendix B. Thermal function $R_T(y,u)$

According to Sect. 3.3, the effects of inelasticity in the electron-nucleus scattering are described by the thermal function $R_T(y,u)$ given by Eq. (20).

Integrating over u we obtain

$$\int_0^\infty \mathrm{d}u\, R_T(y,u) \;=\; 1+\frac{2y^2}{1-y^2}\ln y \rightarrow \begin{cases} 1 & y \ll 1, \\ \frac{1}{2}(1-y^2) & y \rightarrow 1. \end{cases} \tag{B1}$$

In the limits of small and large u we have

$$R_T(y,u)=\frac{63}{160\pi^2}\,u\frac{1-y^2}{y^2}, \quad \text{for } y^2 \gg u, \tag{B2}$$

$$R_T(y,u)=\frac{189}{32\pi^6}\,u^2\mathrm{e}^{-u/2}, \quad \text{for } u\,(1-y^2) \gg 2\,y^2. \tag{B3}$$

If $y \ll 1$, Eq. (20) yields

$$R_T(y,u)\rightarrow R_T(u)=\frac{189}{16\pi^6}\int_{u/2}^\infty \mathrm{d}v\,\frac{v^2}{\mathrm{e}^v-1}\left(v-\frac{u}{2}\right)^2. \tag{B4}$$

The asymptotic forms are:

$$\begin{aligned} R_T(u) &= \frac{189}{16\pi^6}\Gamma(5)\zeta(5) \quad 1 \gg u \gg y^2, \\ R_T(u) &= \frac{189}{32\pi^6}\,u^2\,\mathrm{e}^{-u/2} \quad u \gg 1, \end{aligned} \tag{B5}$$

where $\zeta(x)$ is the zeta function. Finally, for $(1-y) \ll 1$ we have

$$R_T(y,u) \approx \frac{189}{16\pi^6}\,(1-y)\,u \times \int_{u/2}^\infty \mathrm{d}v\,\frac{v^2}{\mathrm{e}^v-1}\,(v-\frac{u}{2}). \tag{B6}$$

We have calculated $R_T(y,u)$ numerically for wide ranges of y and u (10 points of y from y=0 to 0.9; 10 points of u from u=0.1 to 30). We have found the following fitting expression

$$\begin{aligned} R_T(y,u) &= u(1-y^2)\,\frac{1+0.5186y^2}{u+2.608y^2}\,\frac{F}{G}, \\ F &= 0.3058+4.331y^2+F_1 u\,\mathrm{e}^{u/2}, \\ G &= 1+58.05y^2+G_1 u\,\mathrm{e}^u, \\ F_1 &= 2.949-2.963y^2+uF_2, \\ F_2 &= 0.7184-0.8565y^2+0.06019u \\ &+ 0.07671y^2u-0.0007771u^2y, \\ G_1 &= 9.797-6.502y^2. \end{aligned} \tag{B7}$$

The mean error of the fit is 3.6%, and the maximum error of 8.1% takes place at y=0.5 and u=4. This expression has been used in calculations presented in Sect. 3.5.

Appendix C: Dynamic screening

In principle, the ion screening of the Coulomb interaction can be dynamic. For a strongly coupled plasma of ions ($\Gamma \gtrsim 1$), the dynamic screening can be introduced through the dynamic structure factor $S(q,\Omega)$ which satisfies the relationship

$$S(q)=\int_{-\infty}^{+\infty}\frac{\mathrm{d}\Omega}{2\pi}\,S(q,\Omega). \tag{C1}$$

Here, $\hbar\Omega$ is the energy transferred from electrons to nuclei. Typical frequencies Ω of the dynamic response are $\Omega \sim \omega_p$, where $\omega_p=\sqrt{4\pi Z^2e^2n_i/m_i}$ is the ion plasma frequency, and m_i is the ion mass. One can see that $\hbar\omega_p/k_\mathrm{B} \lesssim T_m \ll T_\mathrm{F}$ in dense stellar matter under consideration. In order to include the dynamic screening, we introduce Ω into the energy conserving delta function in Eq. (A1), and rewrite the static structure factor $S(q)$ in the form (C1). Then the Coulomb logarithm for the relativistic degenerate electrons reads (cf. Eq. (14))

$$L \;=\; \frac{189}{2^{11}\pi^9T^6}\int_{-\infty}^{+\infty}\frac{\mathrm{d}\Omega}{2\pi}\int \mathrm{d}\mathbf{k}\,\mathrm{d}\mathbf{p}\,\mathrm{d}\mathbf{p}'\,\frac{S(q,\Omega)|F(q)|^2}{\varepsilon\varepsilon' q^4|\epsilon(q)|^2} \times\; f(1-f')\,\omega J_+. \tag{C2}$$

This equation can be simplified as in Sect. 3.3. Let us introduce the same quantities $\mathbf{q}=\mathbf{q}_t+\mathbf{q}_r$, $\mathbf{k}=\mathbf{k}_t+\mathbf{k}_r$ and $\mathbf{p}''=\mathbf{p}-\mathbf{q}_t=\mathbf{p}'+\mathbf{k}+\mathbf{q}_r$, where $|\mathbf{p}''|=|\mathbf{p}|$. Using energy-momentum conservation and the inequalities $k \ll p$, $q_r \ll p$ we obtain

$$\begin{aligned} \Omega+\omega &\approx q_r+k_r \\ u &= 2P'K+K^2 \approx 2p(\omega-k_r)=2p(q_r-\Omega), \\ v &= 2PK-K^2 \approx 2p(q_r-\Omega-\mathbf{q}_t\mathbf{k}/p), \\ K^2 &= \omega^2-k_r^2-k_t^2 \approx k_0^2-k_t^2. \end{aligned} \tag{C3}$$

Here $k_0^2=(q_r-\Omega)(2\omega-q_r+\Omega)$, and the condition $K^2>0$ yields $2\omega > q_r-\Omega > 0$. If $q \approx q_t$ and q is much larger than q_r, Ω and ω, we have (cf. Eq. (A14))

$$J_+ \approx \frac{8(k_0^2-k_t^2)q_t^2}{(q_r-\Omega)(q_r-\Omega-\mathbf{q}_t\mathbf{k}/p)}\left(1-\frac{q_t^2}{4p^2}\right). \tag{C4}$$

On the other hand, using the approximation of small-angle scattering ($q \ll p$) and (A16), we obtain (cf. Eq. (A15))

$$J_+ \approx \frac{8(k_0^2-k_t^2)}{(q_r-\Omega)^2}\left[q_t^2+2\Omega(q_r-\Omega)\right]. \tag{C5}$$

Combining Eqs. (C4) and (C5), we can propose the following interpolation

$$J_+ \;\approx\; \frac{8(k_0^2-k_t^2)}{(q_r-\Omega)(q_r-\Omega-\mathbf{q}_t\mathbf{k}/p)}\left(1-\frac{q_t^2}{4p^2}\right) \times\; \left[q_t^2+2\Omega(q_r-\Omega)\right]. \tag{C6}$$

Calculations similar to those in Sect. 3.3 allow us to express L in the form analogous to (19). Using (C6), we come to a simple equation for the Coulomb logarithm:

$$L \;=\; \int_{-\infty}^{+\infty}\frac{\mathrm{d}\Omega}{2\pi}\int_0^{2p_F}\mathrm{d}q_t\,q_t\int_\Omega^\infty\frac{\mathrm{d}q_r}{T}\,[q_t^2+2\Omega(q_r-\Omega)] \times\; \frac{S(q,\Omega)|F(q)|^2}{q^4|\epsilon(q)|^2}R_T(y,u,w)R_{NB}(q_t). \tag{C7}$$

Here $q = \sqrt{q_t^2 + q_r^2 - q_t^2(q_r/p)}$, and we introduce a new function

$$
\begin{aligned}
R_T(y,u,w) \;=\; & \frac{189}{16\pi^6}\left\{\int_{v_0}^{v_1} \mathrm{d}v\, \frac{v(v+w)(v-v_0)^2}{\mathrm{e}^{v+w}-1}\right. \\
& \times \left[1 - \frac{v-v_0}{3v_1(1-y^2)}\right] \\
& +\; v_1(1-y^2)\int_{v_1}^{\infty} \mathrm{d}v\, \frac{v(v+w)}{\mathrm{e}^{v+w}-1} \\
& \times \left.\left[v - v_0 - \frac{1}{3}v_1(1-y^2)\right]\right\}, \qquad \text{(C8)}
\end{aligned}
$$

with $y = q_t/(2p_F)$, $u = q_r/T$, $w = \Omega/T$, $v = \omega/T$, $v_0 = (u-w)/2$ and $v_1 = v_0/y^2$. This function describes the thermal effects (Sect. 3.3) in the presence of the dynamic screening. Eq. (C8) yields

$$
\begin{aligned}
& \int_0^\infty \mathrm{d}u' R_T(y, w+u', w) = \\
& R_c(y)\,\frac{63}{8\pi^6}\int_0^\infty \mathrm{d}v \frac{v^4(v+w)}{\mathrm{e}^{v+w}-1}, \qquad \text{(C9)}
\end{aligned}
$$

where $R_c(y)$ is defined by (22). Consider the low-temperature case ($T \ll q_s$) and take into account that $R_T(y,u,w)$ decreases exponentially with increasing $(q_r - \Omega)$ at $(q_r - \Omega) > T$ (see Sect. 3.4). Then Eq. (C7) reduces to

$$
\begin{aligned}
L \;=\; & \frac{63}{8\pi^6}\int_0^{2p_F} \mathrm{d}q_t\, q_t^3\, \frac{|F(q)|^2 R_c(y) R_{\rm NB}(q_t)}{q^4|\epsilon(q)|^2} \\
\times & \int_{-\infty}^{\infty} \frac{\mathrm{d}\Omega}{2\pi} S(q,\Omega) \int_0^\infty \mathrm{d}v \frac{v^4(v+w)}{\mathrm{e}^{v+w}-1}. \qquad \text{(C10)}
\end{aligned}
$$

Let us assume further that the dynamic structure factor $S(q,\Omega)$ decreases rapidly with the growth of Ω at low Ω. Then we can set $\Omega = 0$ or $w = 0$ everywhere in the integrand of (C7) or (C10) except in $S(q,\Omega)$. In this way we have $R_T(y,u,w) = R_T(y,u)$ (cf. (20) and (C8)). The integration over Ω yields the static structure factor $S(q)$ in accordance with (C1), and the Coulomb logarithm (C7) transforms into the static Coulomb logarithm (19).

Thus Eq. (C7) extends the results of Sect. 3.3 to the case of the dynamic screening. In the latter case the Coulomb logarithm is given by a three dimensional integral which could be computed if the dynamic structure factor were known. However the detailed calculations of $S(q,\Omega)$ have not yet been performed. We expect that the formalism will be useful in the future after $S(q,\Omega)$ is determined. Our preliminary estimates indicate that the dynamic effects are not very significant.

References

Berestetskii, V.B., Lifshitz, E.M., Pitaevskii, L.P. 1982, Quantum Electrodynamics, Pergamon, Oxford

Burrows, A., Lattimer, J.M. 1984, ApJ, 285, 294

Cazzola, P., De Zotti, G., and Saggion, A. 1971, Phys. Rev., D3, 1722

Chabrier, G. 1993, ApJ, 414, 695

Dicus, D.A., Kolb, E.W., Schramm, D.N., Tubbs, D.L. 1976, ApJ, 210, 481

Doggett, J.A., Spencer, L.V. 1956, Phys. Rev., 103, 1579

Festa, G.G., Ruderman, M.A. 1969, Phys. Rev., 180, 1227

Flowers, E. 1973, ApJ, 180, 911

Haensel, P., Zdunik, J.L., Dobaczewski, J. 1989, A&A, 222, 353

Haensel, P., Zdunik, J.L. 1990, A&A, 229, 117

Haensel, P., Pichon, B. 1994, A&A, 283, 313

Ichimaru, S., Iyetomi, H., Mitake, S., Itoh, N. 1983, ApJ (Letters), 265, L83

Itoh, N., Kohyama, Y., 1983, ApJ 275, 858

Itoh, N., Mitake, S., Iyetomi, H., Ichimaru, S. 1983, ApJ 273, 774

Itoh, N., Matsumoto, N., Seki, M., Kohyama, Y. 1984a, ApJ, 279, 413

Itoh, N., Kohyama, Y., Matsumoto, N., Seki, M. 1984b, ApJ, 285, 304

Itoh, N., Adachi, T., Nakagawa, M., Kohyama, Y., Munakata, H. 1989, ApJ, 339, 354; Erratum: 1990, ApJ, 360, 741

Jancovici, B., 1962, Nuovo Cim., 25, 428

Lattimer, J.M., Swesty, F.F. 1991, Nucl. Phys. A535, 331

Lattimer, J.M., Van Riper, K., Prakash, M., Prakash, M. 1994, ApJ, 425, 802

Lorenz, C.P., Ravenhall, D.G., Pethick, C.J. 1993, Phys. Rev. Lett., 70, 379.

Miralda-Escudé, J., Haensel, P., Paczyński, B. 1990, ApJ, 362, 572

Mochkovitch, R., Hansen, J.-P. 1979, Phys. Lett., A73, 35

Munakata, H., Kohyama, Ya., Itoh, N. 1987, ApJ, 316, 708

Nagara, H., Nagata, Y., Nakamura, T. 1987, Phys. Rev., A36, 1859

Negele, J.W., Vautherin, D. 1973, Nucl. Phys., A207, 298

Pethick, C.J., Thorsson, V. 1994, Phys. Rev. Lett., 72, 1964

Shapiro, S.L., Teukolsky, S.A. 1983, Black Holes, White Dwarfs and Neutron Stars, Wiley, New York

Soyeur, M., Brown, G.E. 1979, Nucl. Phys., A324, 464

Yakovlev, D.G., Kaminker, A.D. 1996, Astron. Lett., to be published

This article was processed by the author using Springer-Verlag LaTeX A&A style file *L-AA* version 3.